Changes in Summer Persistent Precipitation over the Middle–Lower Reaches of the Yangtze River and Associated Atmospheric Circulation Patterns

Rong YU and Panmao ZHAI*

State Key Laboratory of Severe Weather, *Chinese Academy of Meteorological Sciences*, *China Meteorological Administration*, *Beijing* 100081

(Received November 5, 2020; in final form March 23, 2021)

ABSTRACT

Persistence is an important property of precipitation and its related impacts. However, changes in persistent precipitation and the possible underlying mechanisms in the context of global warming have not yet been discussed in sufficient depth. In this study, the changes in persistent precipitation in summer and related atmospheric circulation patterns over the middle–lower reaches of the Yangtze River (MLRYZR)—a typical monsoon region frequently hit by consecutive rainfall events—are analyzed based on observed daily precipitation and NCEP/NCAR reanalysis data from 1961 to 2019. The results reveal that persistent precipitation events (PPs) tend to happen in a more persistent way, with increased frequency and intensity in the MLRYZR region. Mechanism analyses show that persistent precipitation has happened along with simultaneous enhancement of some large-scale atmospheric circulation patterns, including the Lake Baikal blocking (BB), the Okhotsk Sea blocking (OB), and the western Pacific subtropical high (WPSH). Such enhanced anomalous circulation patterns could persistently reinforce the convergence and supply of water vapor in the MLRYZR region, contributing to the increase in PPs in this region. Based on the above results, we are able to offer some new insights into the long-term changes in precipitation structure and the possible causes. This study is also expected to support attribution studies on regional precipitation changes in the future.

Key words: persistent precipitation, precipitation change, atmospheric circulation pattern

Citation: Yu, R., and P. M. Zhai, 2021: Changes in summer persistent precipitation over the middle–lower reaches of the Yangtze River and associated atmospheric circulation patterns. *J. Meteor. Res.*, **35**(3), 393–401, doi: 10.1007/s13351-021-0186-z.

1. Introduction

Many previous studies have detected significant changes in precipitation in different regions of the world (Emori and Brown, 2005; Toreti et al., 2009; de los Milagros et al., 2013; Du et al., 2019; Han et al., 2019). In China, studies on changes in the number of rainy days (RDs), the intensity of precipitation, and the amount of precipitation have revealed obvious regional patterns (Zhai et al., 2005; Day et al., 2018; Sun and Wang, 2018; Yin et al., 2020). Precipitation persistence is also an important property of precipitation, which is closely related to its impacts (Zolina et al., 2013; Chen and Zhai, 2014a). For example, in 2020, several widespread persistent precipitation events (PPs) occurred during the Meiyu period in the middle–lower reaches of the Yangtze River (MLRYZR; Liu and Ding, 2020), which imposed substantial impacts on people's livelihoods, regional economies, and even the death toll, due to the large-scale floods and geological disasters induced.

An increasing number of studies are being conducted, in which precipitation persistence is analyzed on the daily timescale. Generally, temporal evolution of the frequency and intensity of precipitation events with a certain duration has been investigated based on persistent rainy days (Bai et al., 2007; Zhang et al., 2012; Guilbert et al., 2015). Recently, based on the contribution of RDs with different durations, it is found that precipitation persistence in Europe has prolonged since the 1950s (Zolina et al., 2010). Such a kind of studies on the changing structure of precipitation persistence have provided an-

Supported by the National Natural Science Foundation of China (41905083) and National Key Research and Development Program of China (2018YFC1507700).

*Corresponding author: pmzhai@cma.gov.cn

other perspective on changes in precipitation properties, in addition to frequency and intensity. Typically influenced by the East Asian summer monsoon, the MLRYZR, which is the most populated and economically developed region in China, is always hit hard by PPs (He and Zhai, 2018). An interesting question to address is how and why the structure of precipitation has changed in the MLYRZR under the global warming background.

Past investigations from the mechanism perspective tended to focus on studying extreme persistent precipitation in China at the synoptic scale. The findings of these studies suggest that atmospheric circulation anomalies in the mid–high latitudes, such as the blocking near the Ural Mountains, Lake Baikal, and Okhotsk Sea; and the South Asian high, as well as the western Pacific subtropical high (WPSH) at low latitudes, are key circulation systems for persistent extreme precipitation events in the MLRYZR region (Tao et al., 2004; Hu et al., 2010; Li and Zhang, 2014). These circulation systems maintain the necessary conditions, such as water vapor convergence and vertical motion, for persistent precipitation in this region (Wang et al., 2019; Chen B. et al., 2020). Thus, synoptic analyses have revealed that persistent extreme precipitation events can always be linked to anomalous large-scale atmospheric circulation patterns (Chen and Zhai, 2014b).

However, from the perspective of long-term change, understanding of the changes in the structure of precipitation is still limited for the Asian monsoon regions. Also, knowledge gaps exist regarding the possible mechanisms of persistent precipitation in relation to key large-scale circulation pattern changes and the attribution of human influence. In this study, firstly, the changes in the structure of precipitation, along with the frequency, intensity, and total precipitation amount, are investigated over the MLRYZR region on the basis of daily precipitation data from 1961 to 2019. The detailed changes are described in Section 3. Then, mechanism analyses linking the changes to the variations of the large-scale atmospheric circulation patterns are carried out, and the results are reported in Section 4. Finally, main conclusions and further discussion are given in Section 5.

2. Data and statistical methods

A daily precipitation dataset comprising observations at 2415 meteorological stations in China during 1961–2019, provided by the National Meteorological Information Center, China Meteorological Administration, was employed in this study. This dataset has been processed with strict quality control and widely used in precipitation-related studies in China (Xu et al., 2013). Further quality control was also applied here to improve the reliability of the results. Specifically, stations were ultimately retained only if they met the criteria outlined in Chen and Zhai (2014a). Following all the quality control procedures, 245 stations in the MLRYZR region (26°–32°N, 111°–123°E) were selected.

To explore the mechanism underlying the changes in precipitation persistence, the NCEP/NCAR (Kalnay et al., 1996) daily reanalysis data at a horizontal resolution of 2.5° × 2.5° were used. The variables in this dataset include the horizontal wind speed, specific humidity, and geopotential height. Here, the geopotential height field was processed into an anomaly field with the global mean subtracted to remove the manifestation of the global-scale rise in geopotential height under global warming (Wu and Wang, 2015). Then, the 500-hPa geopotential height anomalies larger than 10 gpm (relative to 1961–2019) in certain regions were defined as anomalous highs (AHs). Additionally, the time series of the summer (June–July–August) Niño index [3-month running mean of ERSST.v5 SST (Extended Reconstructed Sea Surface Temperature version 5) anomalies in the Niño-3.4 region (5°S–5°N, 120°–170°W)] was obtained from the Climate Prediction Center of NCEP (https://origin.cpc.ncep.noaa.gov/products/analysis_monitoring/ensostuff/ONI_v5.php) and applied in this study.

In this study, when daily precipitation was greater than 0.1 mm, that day was defined as an RD. If an RD persisted for m days, it was regarded as an m-day precipitation event. The precipitation event was considered as having ended as soon as the daily precipitation did not meet the threshold. To analyze the precipitation structure in summer for the period from 1961 to 2019, precipitation events were classified into five categories of persistence from 1 to 5 days. Here, precipitation events with duration longer than 5 days were sorted into the 5-day category. Following the process outlined in Zolina et al. (2010), the contribution of precipitation events with m days was calculated as

$$F\left(X_{i,j,m}\right) = \mathrm{Td}_{i,j,m}/\mathrm{Td}_{i,j} \quad (i = 1,2,...,2415; \; j = 1961,1962,...,2019; m = 1,2,...,5), \tag{1}$$

where $\mathrm{Td}_{i,j,m}$ refers to the total number of RDs for station i, year j, and category m, while $\mathrm{Td}_{i,j}$ refers to total number of RDs for station i and year j. If the contribution of precipitation events with m days is increased, it means that precipitation events have tended to happen in m days. Then, following the results of changes in persistence structure, precipitation events are classified as PPs and non-PPs (NPPs): a PP is defined as a precipitation

event with duration of at least 2 days; and an NPP is defined as a precipitation event with duration of 1 day. If the contribution of PPs is increased, it means that the precipitation structure has changed to one with a greater occurrence of PPs.

Principal Component Analysis (PCA; Abdi and Williams, 2010) was applied to provide information on the spatiotemporal variations of key circulation systems and persistent precipitation. Based on this analysis, the associations between changes in persistent precipitation and related large-scale circulation systems from 1961 to 2019 were evaluated. Moreover, the Mann–Kendall test, which is a non-parametric (i.e., distribution-free) test, was used to detect the presence of linear trends in related time series, and the Theil–Sen robustness test was applied to estimate the significance levels in the linear trends (Mondal et al., 2012). Pearson's correlation coefficient was adopted to calculate the correlations in this study.

3. Changes in precipitation properties

Based on the most-updated daily precipitation observations in China, spatial distributions of the trends in the total precipitation amount, intensity, and frequency of RDs from 1961 to 2019 are displayed in Fig. 1a. As shown, the total precipitation has widely and significantly increased in the MLRYZR region. The intensity of precipitation has universally increased in the study region. Meanwhile, the frequency of RDs has also increased, except in some parts of the northwestern MLRYZR region. Decreasing trends are only apparent in a small part of the northwestern MLRYZR region, which is a transition area under the influence of the East Asian monsoon. This is possibly due to a regional response to the change in the East Asian summer monsoon system against the global warming background (Zhai et al., 2005). Overall, the regionally averaged frequency and intensity of precipitation in the MLRYZR region display increasing trends of 0.4 day (10 yr)$^{-1}$ and 0.6 mm (day 10 yr)$^{-1}$, respectively (Fig. 1b). More frequent and intensified precipitation events have been detected in the MLRYZR region.

The change in regionally averaged precipitation persistence is presented in Fig. 2. As shown in Fig. 2a, the change in the contribution of 1-day precipitation events in the MLRYZR region displays a significant decrease at the 99% confidence level. However, the trends in the contribution of 2–5-day precipitation events all present increasing trends—especially for 3- and 4-day precipitation events. The 2–5-day precipitation events are identified as PPs (see Section 2). Thus, the contribution of NPPs has decreased, while that of PPs has increased.

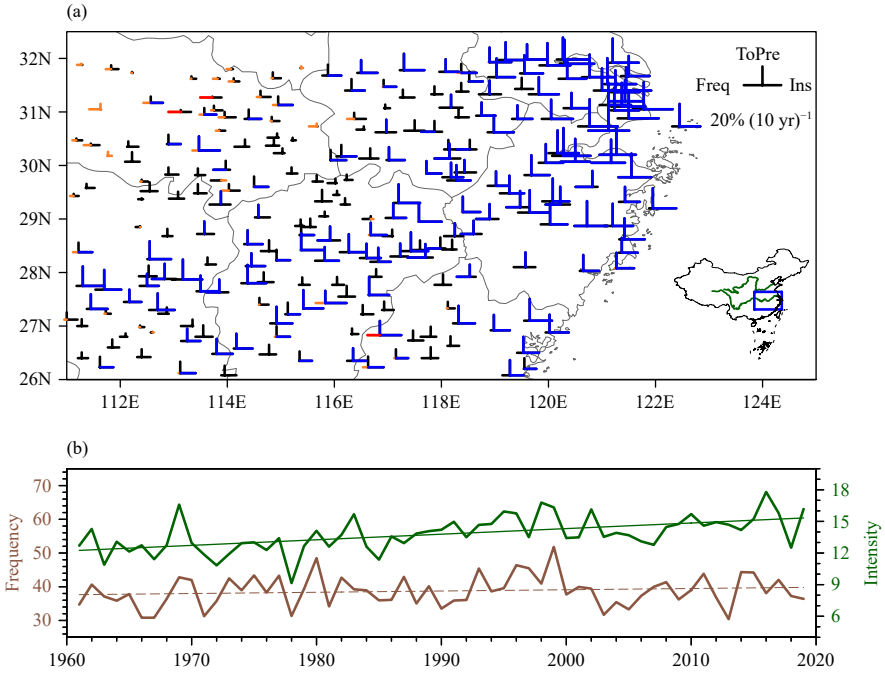

Fig. 1. (a) Spatial distribution of the trend [% (10 yr)$^{-1}$] in the total precipitation (ToPre), frequency (Freq), and intensity (Ins) of summer RDs. The black bars refer to stations with increasing trends for total precipitation, frequency, and intensity, while the orange bars refer to stations with decreasing trends. Blue/red bars refer to stations with significant increasing/decreasing trends for total precipitation at the 90% confidence level. (b) Time series of averaged frequency (brown line) and intensity (green line) of RDs for all stations in the MLRYZR region for the summers of 1961–2019.

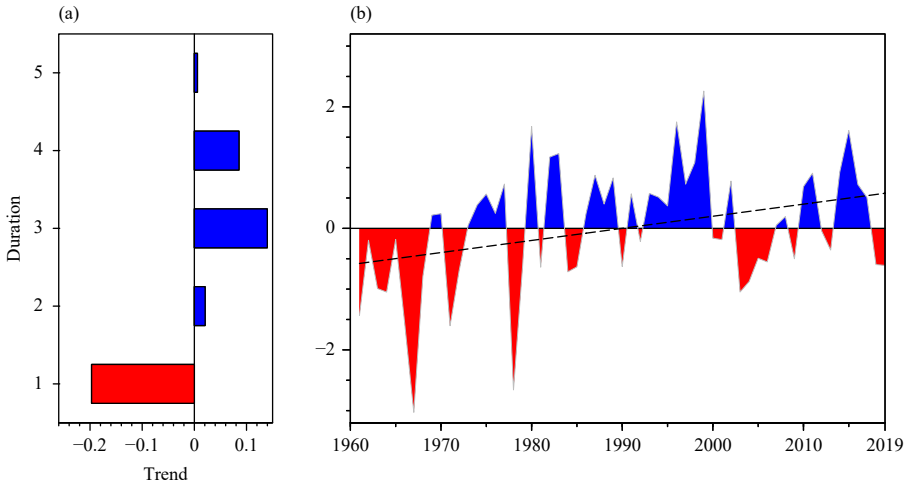

Fig. 2. Trends [x-axis; (10 yr)$^{-1}$] of (a) the normalized occurrence anomalies (relative to 1961–2019) of the contribution of precipitation events with different durations (y-axis; day) to the total numbers of RDs, and (b) normalized (relative to 1961–2019) temporal evolution (shaded) for the contribution of PP days to the summers from 1961 to 2019 in the MLRYZR region. The black dashed line in (b) refers to the corresponding linear regression.

From this perspective, precipitation tends to happen in the form of PPs in the MLRYZR region.

As for the temporal evolution (Fig. 2b), the contribution of PPs was generally below normal before 1970, but since then it has mainly been above normal, except for some years in the 2000s. Although some different timescales of variability exist in the contribution of PPs during 1961–2019, an increasing trend of 0.2 (10 yr)$^{-1}$ is statistically significant at the 99% confidence level. Spatially, the contribution of PPs has increased significantly at a rate of over 1% (10 yr)$^{-1}$ (at the 95% confidence level) in the MLRYZR region (Fig. 3), especially in some areas along the Yangtze River. This suggests that the persistence of precipitation events in the MLRYZR region has restructured in the summers from 1961 to 2019. Thus, a new result is that precipitation events tend to happen in a more persistent way along with increased frequency and intensity.

4. Related circulation changes

To reveal the mechanism underlying the increase in persistent precipitation in the MLRYZR region, changes in PPs related large-scale circulation systems at the daily timescale were analyzed based on the following steps. Firstly, the composite large-scale circulation anomalies during widespread concurrent PPs were diagnosed in the study region for the period 1961–2019. Then, possible spatial linkages between the diagnosed key circulation systems at 500 hPa and the PPs were studied by using

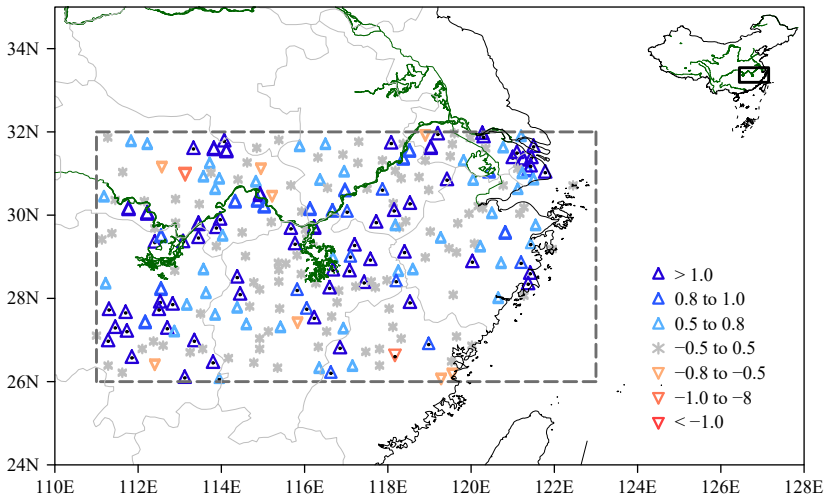

Fig. 3. Spatial distribution of the trend [% (10 yr)$^{-1}$)] in the contribution of the total number of PP days to the total number of RDs in summer of 1961–2019. The stations with a black dot inside refer to the stations with a trend at the 90% confidence level.

PCA. Finally, based on the main component of the PCA results, the changes in related key circulation patterns were analyzed to reveal possible causes for changes in PPs.

4.1 *Connecting PP changes to daily circulation systems*

Previous studies have indicated that circulation systems in the mid–high latitudes, such as the Ural blocking (UB), Lake Baikal blocking (BB), and Okhotsk Sea blocking (OB), as well as the WPSH in the low latitudes, are key systems for certain persistent extreme precipitation events in the MLRYZR region (Chen and Zhai, 2014b). These circulation systems are related to water vapor transport and vertical air motion, which are necessary condition for precipitation (Wang et al., 2019; Chen B. et al., 2020).

In order to connect the large-scale circulation with the PPs at the daily scale, widespread concurrent PPs were identified based on PPs covering at least 40% of the stations in the study region (Zhang et al., 2005). To justify the rationality of using a spatial coverage of 40% as the threshold, other thresholds, such as 30% and 50%, were also tested and the results confirmed that the selection of the 40% threshold was appropriate. The concurrent large-scale circulation anomalies of such events were investigated through composite analysis. As shown in Fig. 4, spatial distributions of the composite 700-hPa horizontal wind anomalies, 500-hPa geopotential height anomalies (Fig. 4a), and related water vapor flux anomalies and precipitable water anomalies (Fig. 4b) are depicted for the widespread concurrent PPs. Clearly, anticyclonic anomalous systems are manifested near the northwestern Pacific Ocean, Lake Baikal, and the Okhotsk Sea (Fig. 4).

Consequently, an enhanced and westerly-extended WPSH is favorable for transporting warm and moist water vapor into the MLRYZR region (Figs. 4b, 5). Meanwhile, strengthened blocking systems near Lake Baikal and the Okhotsk Sea seem to bring persistently cold and dry air flux into the MLRYZR region (Figs. 4b, 5). Accordingly, an anomalous cyclonic circulation is clearly seen over the MLYRZR region. Such cyclonic anomalies have contributed to converging more water vapor, bringing more cold and dry air flow from higher latitudes, and concurrently promoting stronger vertical motion in this region (Fig. 4). As a result, these anomalous circulation systems have jointly led to widespread concurrent PPs in the MLRYZR region.

As stated earlier, PPs that occur in the MLRYZR region are dominated by the influence of these AH–pressure circulation systems. To better reveal the key circulation systems influencing the occurrence of PPs, correlation analyses were conducted between the occurrence of much-above-normal geopotential height at 500 hPa (AH) and the contribution of PPs. As indicated in Fig. 5, significant high-correlation areas are also apparent near Lake Baikal, the Okhotsk Sea, and the northwestern subtropical Pacific Ocean. Based on Figs. 4, 5, BB (40°–60°N, 50°–80°E), OB (55°–68°N, 112°–145°E), and WPSH (15°–25°N, 105°–135°E) are identifiable as the key circulation systems. It is revealed that the averaged PPs in the MLRYZR region are highly related to the occurrence of enhanced BB and OB, and a strengthened WPSH.

4.2 *Identifying key influencing circulation patterns*

To further investigate the spatial synergy among these key AH–pressure circulation systems and persistent pre-

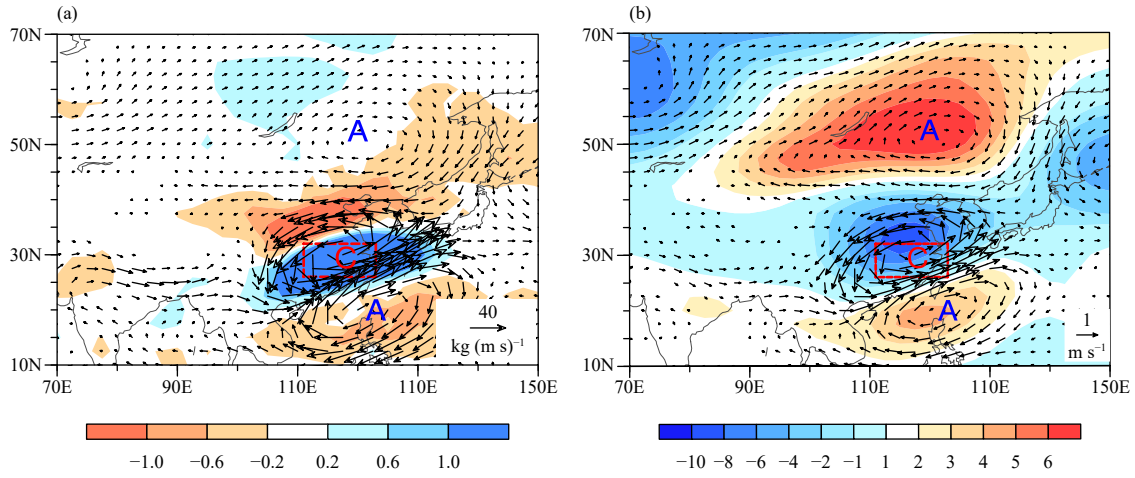

Fig. 4. Composite fields of (a) water vapor flux [vector; kg (m s)$^{-1}$] and precipitable water (shading; kg m^{-2}) anomalies, and (b) 700-hPa horizontal wind (vector; m s^{-1}) and 500-hPa geopotential height (shading; gpm) anomalies for the days identified as having widespread concurrent PPs relative to 1961–2019. Red box refers to the MLRYZR region. Letters "A" and "C" refer to anticyclone and cyclone anomalies, respectively.

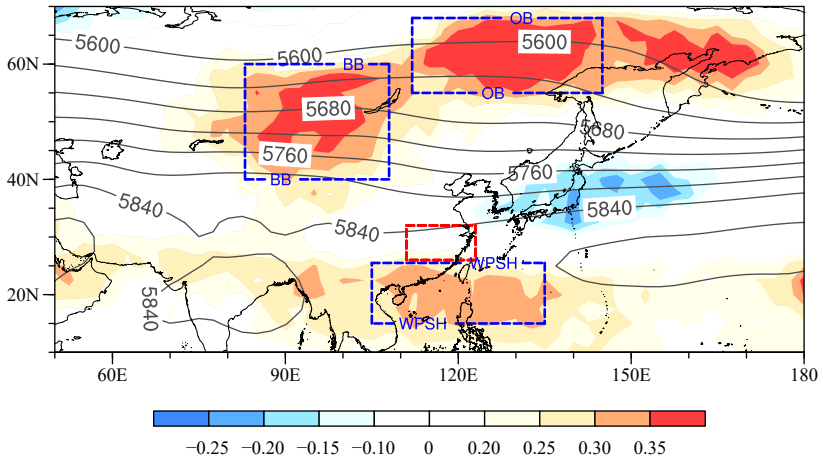

Fig. 5. Spatial distribution of the correlations between the occurrence of anomalous highs (AHs) and the contribution of PPs from 1961 to 2019 (shading). Solid lines refer to the climatological average 500-hPa geopotential height (gpm) of 1961–2019. Blue boxes indicate the areas of Lake Baikal blocking (BB), Okhotsk Sea blocking (OB), and the western Pacific subtropical high (WPSH). The red box refers to the MLRYZR region.

cipitation, PCA was applied to compute the spatiotemporal decomposition. The results show that the contributions of the variances of the first three leading eigenvectors reach up to 68%, 18%, and 13%, respectively. Specifically, the first eigenvector exhibits a uniformly positive spatial pattern reflecting synchronized anomalous circulation systems and precipitation changes (Fig. 6a). It implies that the variation in the increased contribution of PPs in the MLRYZR region is consistent with the variations in the occurrence of a pattern with anomalously developed BB, OB, and WPSH (hereafter referred to as the "BB + OB + WPSH" pattern). Noticeably, the BB + OB + WPSH pattern is closely related to PPs. The second eigenvector suggests that the increased contribution of PPs coincides with the occurrence of enhanced OB and BB, but a weakened WPSH (figure omitted). As for the third eigenvector (figure omitted), the enhanced contribution of PPs is related to an above-normal occurrence of enhanced OB and WPSH, and a below-normal occurrence of an enhanced BB. However, such asynchronous changes in these circulation systems have a limited influence on the contribution of PPs. Generally, a matched BB + OB + WPHS pattern, leading to changes in PPs with a 68% contribution variance, is the main anomalous circulation pattern for PPs in the MLRYZR region. Such synchronous circulation system changes have exerted an important influence on persistent precipitation. As PC1 displays a positive trend (Fig. 6b), this implies that the increase in PPs is mainly influenced by the BB + OB + WPSH pattern.

4.3 *Changes in the key anomalous circulation pattern*

To further understand the changes in the synchronized key circulation systems influencing PPs in the MLRYZR region, time series of the occurrence of a persistent BB + OB + WPSH pattern (persistent for over two days) and the contribution of PPs are illustrated in Fig. 7. As we can see, the occurrence of the key circulation pattern varies coincidently with the contribution of PPs, with a positive correlation of 0.4 at the 95% confidence level. This

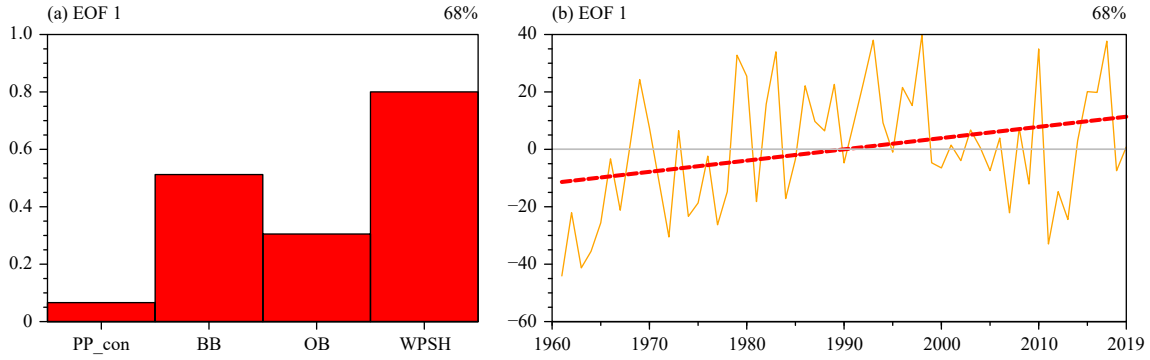

Fig. 6. (a) The first leading eigenvectors and (b) corresponding principal component (PC1) of the contribution of PPs (PP_con) in the MLRYZR region and the occurrence of AHs in BB, OB, and WPSH. The red dashed line in (b) refers to the corresponding linear regression.

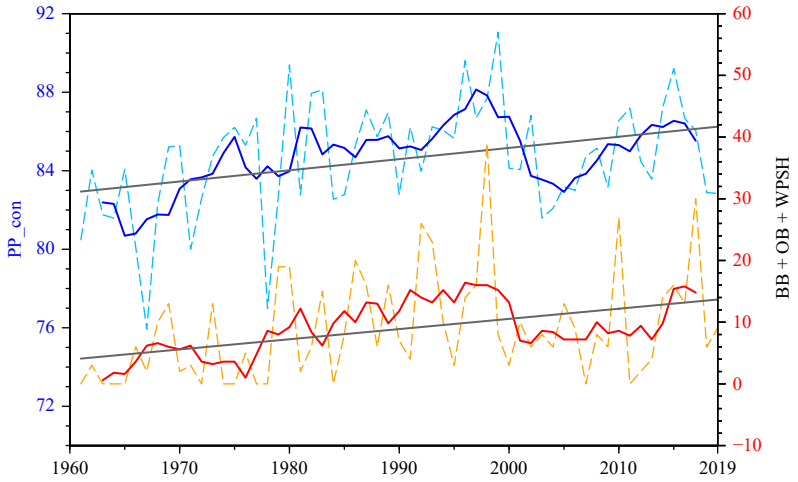

Fig. 7. Time series of the occurrence of a persistent BB + OB + WPSH pattern (persistent for at least 2 days; day) and the contribution of PPs (%) in summer for the period 1961–2019. The blue and red solid lines refer to the corresponding 5-yr running average. The gray solid line refers to the linear regression.

indicates that persistent precipitation is closely connected with this anomalous circulation pattern. Under such a condition, persistent dry and cold flow in association with BB and OB converge in the MLRYZR region with persistent moist and warm air transported from the WPSH, maintaining the water vapor supply and vertical motion. These conditions therefore support the occurrence of PPs in this region. Furthermore, the occurrence of a persistent BB + OB + WPSH pattern has changed with a trend of 1.4 days $(10\ \mathrm{yr})^{-1}$, significant at the 99% confidence level. Thus, precipitation in the MLRYZR region has restructured in the form of more PPs, which is possibly due to the reinforced persistent BB + OB + WPSH pattern.

Yao and Ren (2019) indicated that interannual and interdecadal variations are important characteristics for persistent heavy rainfall. Here, as we can see from Fig. 7, related variation also exists in the contribution of PPs. To explore the possible causes, further analysis was applied to the detrended time series for the key circulation pattern and the contribution of PPs. It was found that these two detrended series are significantly correlated, with a correlation of 0.3. Clearly, the variability of the BB + OB + WPSH pattern also influences the variation of persistent precipitation in the MLRYZR region on interannual and interdecadal timescales.

It has been recognized that in El Niño years, both the blocking at high latitudes and the WPSH at low latitudes are enhanced due to the anomalies in the sea surface thermal condition and air–sea interactions (Feng et al., 2011; Wang et al., 2012; Li et al., 2016; Yu and Zhai, 2018), which ultimately promotes precipitation to occur in a more persistent way in the MLRYZR region. Further analyses support the fact that tropical SST anomalies could influence the BB + OB + WPSH pattern, as we found that the summer Niño index is significantly correlated with this pattern (correlation of 0.3). Besides, a shift in the Pacific Decadal Oscillation (PDO) can also result in changes to the summer precipitation pattern in East China via warming over Lake Baikal and a weakening of the westerly jet (Zhu et al., 2011).

5. Conclusions and discussion

In this study, the changes in the structure of summer precipitation in the MLRYZR region and the possible mechanisms linking them to key large-scale circulation system changes were investigated based on daily observations and reanalysis data from 1961 to 2019. Overall, this diagnostic study provides a more comprehensive understanding of the changes in precipitation that have taken place in the MLRYZR region in recent decades. More specifically, the main conclusions are as follows.

(1) Precipitation events in the MLRYZR region have tended to occur in the form of more PPs along with increased intensity and frequency. The contribution of NPPs has decreased significantly, while that of PPs has increased. Thus, an increased contribution of persistent precipitation days to all RDs is one of the essential features of recent precipitation change in the MLRYZR region.

(2) Mechanism analysis revealed that a persistently synchronized enhancement of blocking systems and the subtropical high is the likely dominant cause of the increased occurrence of PPs in the MLRYZR region. Under such conditions, dry and cold flow in association

with BB and OB persistently converges in the MLRYZR region with moist and warm air induced by the WPSH, thus maintaining the level of water vapor and vertical motion and ultimately leading to the occurrence of persistent precipitation in this region. Regarding the enhanced BB + OB + WPSH pattern from 1961 to 2019, this is possibly connected with sea-ice loss and subsequent Arctic warming (Cohen et al., 2017; Coumou et al., 2018) linked to the global warming background.

Previous studies have suggested that the WPSH and blocking systems have become more persistent and strengthened during recent decades (Horton et al., 2015; Luo et al., 2016; Tyrlis et al., 2020). Based on further in-depth attribution studies for these circulation systems, changes in blocking can be attributed to human influence (Dennison et al., 2015). However, there have yet to be many detection and attribution studies carried out for the combined changes in these circulation systems. In this paper, we have detected the key circulation pattern changes for PPs and discussed their possible linkages. The findings provide a foundation for further studies to facilitate storyline attribution of persistent precipitation from the circulation perspective. Also, many studies have provided information on the projected changes in precipitation in the MLRYZR region by using several methods (Wu et al., 2016; Yu et al., 2018). Noticeably, the WPSH and mid–high-latitude blocking are projected to become more persistent according to some studies (Mokhov et al., 2014; Chen X. L. et al., 2020). Therefore, future precipitation changes in the MLRYZR region are worthy of further study in terms of their connection with the projected changes in the dominant circulation systems.

REFERENCES

Abdi, H., and L. J. Williams, 2010: Principal component analysis. *WIREs Comput. Stat.*, **2**, 433–459, doi: 10.1002/wics.101.

Bai, A. J., P. M. Zhai, and X. D. Liu, 2007: Climatology and trends of wet spells in China. *Theor. Appl. Climatol.*, **88**, 139–148, doi: 10.1007/s00704-006-0235-7.

Chen, B., W. Zhang, S. Yang, et al., 2020: Roles of oceanic moisture exports in modulating summer rainfall over the middle-lower Yangtze River Basin: Inter-annual variability and decadal transition. *Int. J. Climatol.*, **40**, 3757–3770, doi: 10.1002/joc.6426.

Chen, X. L., T. J. Zhou, P. L. Wu, et al., 2020: Emergent constraints on future projections of the western North Pacific Subtropical High. *Nat. Commun.*, **11**, 2802, doi: 10.1038/s41467-020-16631-9.

Chen, Y., and P. M. Zhai, 2014a: Changing structure of wet periods across southwest China during 1961–2012. *Climate Res.*, **61**, 123–131, doi: 10.3354/cr01247.

Chen, Y., and P. M. Zhai, 2014b: Two types of typical circulation pattern for persistent extreme precipitation in Central–Eastern China. *Quart. J. Roy. Meteor. Soc.*, **140**, 1467–1478, doi: 10.1002/qj.2231.

Cohen, J., J. A. Screen, J. C. Furtado, et al., 2017: Recent Arctic amplification and extreme mid-latitude weather. *Nat. Geosci.*, **7**, 627–637, doi: 10.1038/ngeo2234.

Coumou, D., G. Di Capua, S. Vavrus, et al., 2018: The influence of Arctic amplification on mid-latitude summer circulation. *Nat. Commun.*, **9**, 2959, doi: 10.1038/s41467-018-05256-8.

Day, J. A., I. Fung, and W. H. Liu, 2018: Changing character of rainfall in eastern China, 1951–2007. *Proc. Natl. Acad. Sci. USA*, **115**, 2016–2021, doi: 10.1073/pnas.1715386115.

de los Milagros Skansi, M., M. Brunet, J. Sigró, et al., 2013: Warming and wetting signals emerging from analysis of changes in climate extreme indices over South America. *Glob. Planet. Change*, **100**, 295–307, doi: 10.1016/j.gloplacha.2012.11.004.

Dennison, F. W., A. J. McDonald, and O. Morgenstern, 2015: The effect of ozone depletion on the Southern Annular Mode and stratosphere-troposphere coupling. *J. Geophys. Res. Atmos.*, **120**, 6305–6312, doi: 10.1002/2014JD023009.

Du, H. B., L. V. Alexander, M. G. Donat, et al., 2019: Precipitation from persistent extremes is increasing in most regions and globally. *Geophys. Res. Lett.*, **46**, 6041–6049, doi: 10.1029/2019GL081898.

Emori, S., and S. J. Brown, 2005: Dynamic and thermodynamic changes in mean and extreme precipitation under changed climate. *Geophys. Res. Lett.*, **32**, L17706, doi: 10.1029/2005GL023272.

Feng, J., W. Chen, C.-Y. Tam, et al., 2011: Different impacts of El Niño and El Niño Modoki on China rainfall in the decaying phases. *Int. J. Climatol.*, **31**, 2091–2101, doi: 10.1002/joc.2217.

Guilbert, J., A. K. Betts, D. M. Rizzo, et al., 2015: Characterization of increased persistence and intensity of precipitation in the northeastern United States. *Geophys. Res. Lett.*, **42**, 1888–1893, doi: 10.1002/2015GL063124.

Han, J. Y., H. B. Du, Z. F. Wu, et al., 2019: Changes in extreme precipitation over dry and wet regions of China during 1961–2014. *J. Geophys. Res. Atmos.*, **124**, 5847–5859, doi: 10.1029/2018JD029974.

He, B.-R., and P.-M. Zhai, 2018: Changes in persistent and non-persistent extreme precipitation in China from 1961 to 2016. *Adv. Climate Change Res.*, **9**, 177–184, doi: 10.1016/j.accre.2018.08.002.

Horton, D. E., N. C. Johnson, D. Singh, et al., 2015: Contribution of changes in atmospheric circulation patterns to extreme temperature trends. *Nature*, **522**, 465–469, doi: 10.1038/nature14550.

Hu, Y. M., Y. H. Ding, and F. Liao, 2010: A classification of the precipitation patterns during the Yangtze–Huaihe Meiyu period for the recent 52 years. *Acta Meteor. Sinica*, **68**, 235–247, doi: 10.11676/qxxb2010.024. (in Chinese)

Kalnay, E., M. Kanamitsu, R. Kistler, et al., 1996: The NCEP/NCAR 40-year reanalysis project. *Bull. Amer. Meteor. Soc.*, **77**, 437–472, doi: 10.1175/1520-0477(1996)077<0437:TNYRP>2.0.CO;2.

Li, L., and Y. C. Zhang, 2014: Effects of different configurations

of the East Asian subtropical and polar front jets on precipitation during the Mei-Yu season. *J. Climate*, **27**, 6660–6672, doi: 10.1175/JCLI-D-14-00021.1.

Li, X., A. Meshgi, and V. Babovic, 2016: Spatio-temporal variation of wet and dry spell characteristics of tropical precipitation in Singapore and its association with ENSO. *Int. J. Climatol.*, **36**, 4831–4846, doi: 10.1002/joc.4672.

Liu, Y. Y., and Y. H. Ding, 2020: Characteristics and possible causes for the extreme Meiyu in 2020. *Meteor. Mon.*, **46**, 1393–1404, doi: 10.7519/j.issn.1000-0526.2020.11.001. (in Chinese)

Luo, D. H., Y. Q. Xiao, Y. Yao, et al., 2016: Impact of Ural blocking on winter warm Arctic–cold Eurasian anomalies. Part I: Blocking-induced amplification. *J. Climate*, **29**, 3925–3947, doi: 10.1175/JCLI-D-15-0611.1.

Mokhov, I. I., A. V. Timazhev, and A. R. Lupo, 2014: Changes in atmospheric blocking characteristics within Euro-Atlantic region and Northern Hemisphere as a whole in the 21st century from model simulations using RCP anthropogenic scenarios. *Glob. Planet. Change*, **122**, 265–270, doi: 10.1016/j.gloplacha.2014.09.004.

Mondal, A., S. Kundu, and A. Mukhopadhyay, 2012: Rainfall trend analysis by Mann–Kendall test: A case study of northeastern part of Cuttack district, Orissa. *Int. J. Geology.*, **2**, 70–78.

Sun, B., and H. J. Wang, 2018: Interannual variation of the spring and summer precipitation over the three river source region in China and the associated regimes. *J. Climate*, **31**, 7441–7457, doi: 10.1175/JCLI-D-17-0680.1.

Tao, S. Y., X. L. Zhang, and S. L. Zhang, 2004: *A Study on the Disasters of Heavy Rainfalls over the Yangtze River Basin in the Meiyu Period*. China Meteorological Press, Beijing, 192 pp. (in Chinese)

Toreti, A., G. Fioravanti, W. Perconti, et al., 2009: Annual and seasonal precipitation over Italy from 1961 to 2006. *Int. J. Climatol.*, **29**, 1976–1987, doi: 10.1002/joc.1840.

Tyrlis, E., J. Bader, E. Manzini, et al., 2020: On the role of Ural Blocking in driving the Warm Arctic–Cold Siberia pattern. *Quart. J. Roy. Meteor. Soc.*, **146**, 2138–2153, doi: 10.1002/qj.3784.

Wang, X., D. X. Wang, W. Zhou, et al., 2012: Interdecadal modulation of the influence of La Niña events on mei-yu rainfall over the Yangtze River valley. *Adv. Atmos. Sci.*, **29**, 157–168, doi: 10.1007/s00376-011-1021-8.

Wang, X. K., X. Q. Dong, Y. Deng, et al., 2019: Contrasting pre-mei-yu and mei-yu extreme precipitation in the Yangtze River valley: Influencing systems and precipitation mechanisms. *J. Hydrometeor.*, **20**, 1961–1980, doi: 10.1175/JHM-D-18-0240.1.

Wu, D., Z. H. Jiang, and T. T. Ma, 2016: Projection of summer precipitation over the Yangtze–Huaihe River basin using multimodel statistical downscaling based on canonical correlation analysis. *J. Meteor. Res.*, **30**, 867–880, doi: 10.1007/s13351-016-6030-1.

Wu, L. G., and C. Wang, 2015: Has the western Pacific subtropical high extended westward since the late 1970s? *J. Climate*, **28**, 5406–5413, doi: 10.1175/JCLI-D-14-00618.1.

Xu, W. H., Q. X. Li, X. L. Wang, et al., 2013: Homogenization of Chinese daily surface air temperatures and analysis of trends in the extreme temperature indices. *J. Geophys. Res. Atmos.*, **118**, 9708–9720, doi: 10.1002/jgrd.50791.

Yao, R., and X. J. Ren, 2019: Decadal and interannual variability of persistent heavy rainfall events over the middle and lower reaches of the Yangtze River valley. *J. Meteor. Res.*, **33**, 1031–1043, doi: 10.1007/s13351-019-9070-5.

Yin, Y. X., C. Han, G. Y. Yang, et al., 2020: Changes in the summer extreme precipitation in the Jianghuai plum rain area and their relationship with the intensity anomalies of the South Asian high. *Atmos. Res.*, **236**, 104793, doi: 10.1016/j.atmosres.2019.104793.

Yu, R., and P. M. Zhai, 2018: The influence of El Niño on summer persistent precipitation structure in the middle and lower reaches of the Yangtze River and its possible mechanism. *Acta Meteor. Sinica*, **76**, 408–419, doi: 10.11676/qxxb2018.012. (in Chinese)

Yu, R., P. M. Zhai, and Y. Y. Lu, 2018: Implications of differential effects between 1.5 and 2°C global warming on temperature and precipitation extremes in China's urban agglomerations. *Int. J. Climatol.*, **38**, 2374–2385, doi: 10.1002/joc.5340.

Zhai, P. M., X. B. Zhang, H. Wan, et al., 2005: Trends in total precipitation and frequency of daily precipitation extremes over China. *J. Climate*, **18**, 1096–1108, doi: 10.1175/JCLI-3318.1.

Zhang, Q., V. P. Singh, J. T. Peng, et al., 2012: Spatial–temporal changes of precipitation structure across the Pearl River basin, China. *J. Hydrol.*, **440–441**, 113–122, doi: 10.1016/j.jhydrol.2012.03.037.

Zhang, Y. X., P. M. Zhai, and Y. F. Qian, 2005: Variations of Meiyu indicators in the Yangtze–Huaihe River basin during 1954–2003. *Acta Meteor. Sinica*, **19**, 479–484.

Zhu, Y. L., H. J. Wang, W. Zhou, et al., 2011: Recent changes in the summer precipitation pattern in East China and the background circulation. *Climate Dyn.*, **36**, 1463–1473, doi: 10.1007/s00382-010-0852-9.

Zolina, O., C. Simmer, S. K. Gulev, et al., 2010: Changing structure of European precipitation: Longer wet periods leading to more abundant rainfalls. *Geophys. Res. Lett.*, **37**, L06704, doi: 10.1029/2010GL042468.

Zolina, O., C. Simmer, K. Belyaev, et al., 2013: Changes in the duration of European wet and dry spells during the last 60 years. *J. Climate*, **26**, 2022–2047, doi: 10.1175/JCLI-D-11-00498.1.

Tech & Copy Editor: Zhirong CHEN